Supergen

Offshore Renewable Energy

Early Career Researcher Posters and Abstracts Booklet

2026 Annual Assembly

Surnames H-L

UKRI Engineering and Physical Sciences Research Council

Early Career Researcher Posters 2026

Payvand Habibi, University of Strathclyde Advanced Stress Analysis for Optimised Marine Energy Structures (ASAMES)
Payvand Habibi, University of Strathclyde An Integrated Experimental-Computational Framework for Erosion Analysis of Tidal Turbine Blades
Yadong Han, University of Oxford Unsteady hydrodynamic forces on a forced oscillating rotor
Anna Holcombe, University of Exeter Assessing the contribution of VIV to fatigue damage in dynamic power cables
Sam Hughes, University of Edinburgh Reduced-Order Modelling (ROM) of Tidal Turbine Rotor Blade Structures
Jack Lewis, University of Strathclyde Offshore Wind Farm Layout Optimisation using Simplified Geometric Blockage Metrics
Ye Li, University of Southampton Concrete Composites in Marine Environment, FRP-enabled sustainable concrete for durable floating wind structures
Chenying Liu, University of Oxford Origami-Enhanced Dielectric Fluid Generator for Wave Energy Conversion

Advanced Stress Analysis for Optimised Marine Energy Structures (ASAMES)

Payvand Habibi[1], Farhad Abad[2], Saeid Lotfian[1] , Feargal Brennan[1]

[1] Department Of Naval Architecture, Ocean & Marine Engineering (NAOME), Faculty of Engineering, Glasgow, UK; [2] Xodus Group, Glasgow, UK

Introduction: Offshore monopiles operate under harsh conditions where residual stresses from manufacturing and installation significantly influence fatigue performance. Current design approaches remain overly conservative due to limited empirical evidence and increasing costs. This research addresses this gap through the systematic post-mortem analysis of full-scale monopiles with known service history, integrating neutron diffraction, contour method, and strain-gauge-based measurements with validated computational modelling. Comparative analysis with newly manufactured reference sections enables separation of stress origins. Timely within the rapid expansion of offshore wind, this work aims to improve fatigue assessment, optimise design, and support reductions in Levelised Cost of Electricity (LCOE).

ITW Welding Singapore
The Welding of Offshore Wind Monopiles

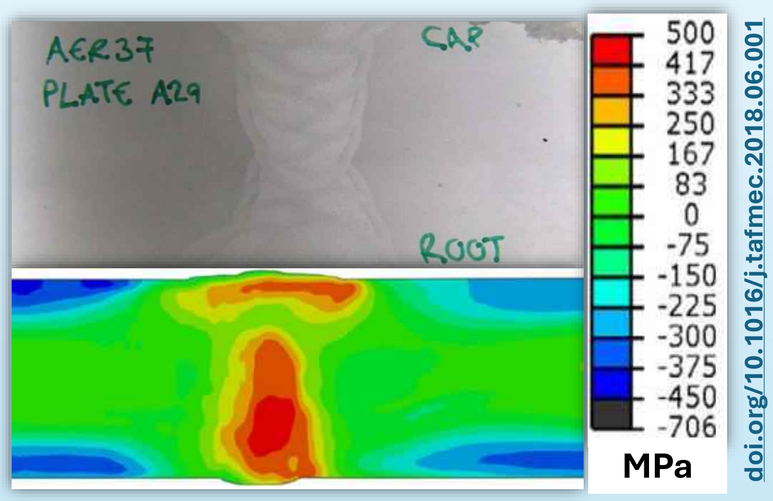

doi.org/10.1016/j.tafmec.2018.06.001

Residual stress measurement (contour method)

Aim & Objectives: The project aims to advance understanding of residual stresses in monopile foundations through integrated experimental and numerical analyses. Key objectives include: (a) *Quantifying residual stress distributions in decommissioned and newly manufactured sections*; (b) *Developing high-fidelity finite element models incorporating manufacturing and installation effects*; (c) *Investigating stress evolution and redistribution mechanisms*; (d) *Enabling parametric studies to support optimised design guidelines*.

The ultimate goal is to improve fatigue life prediction while reducing conservative design margins.

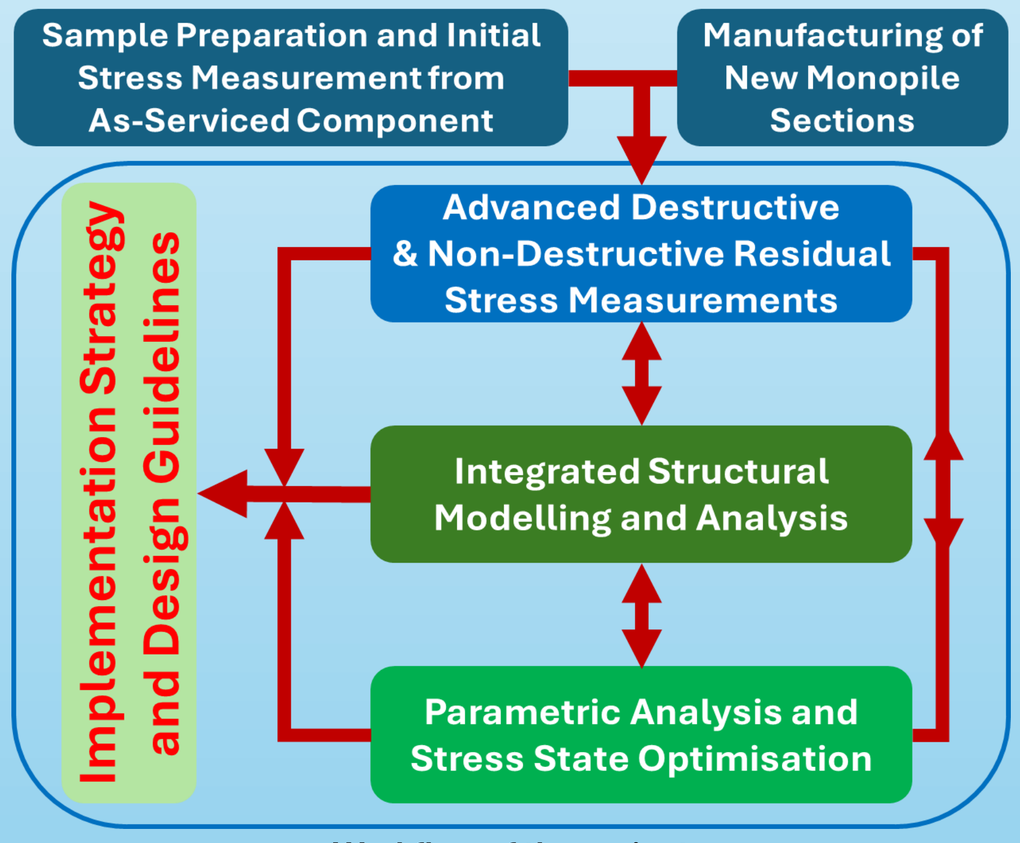

Workflow of the project

Section of the decommissioned monopile

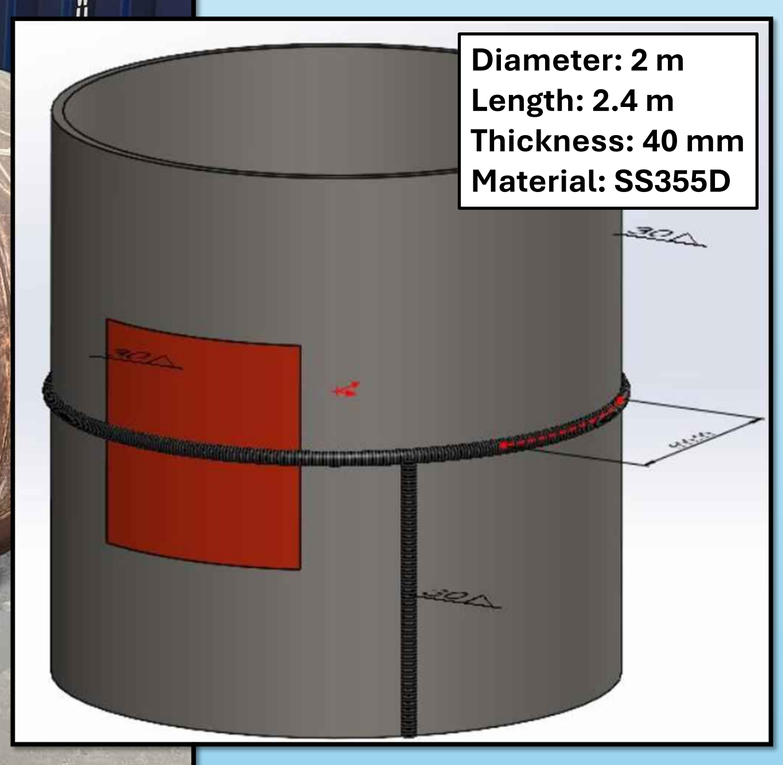

Schematic of the location for the cutting of the welded samples

Initial Results:

- **Stress release** measured using 3-grid strain gauge rosettes (0°/45°/90°), enabling principal stress reconstruction. Multiple gauge locations (SG1–SG5) are used to ensure spatial resolution.
- **Temperature compensation** applied due to high-temperature cutting effects. The measurement illustrates a **measurable drift**, confirming the need for correction models.
- Stress results show **non-uniform residual stress distribution**, particularly **across weld regions**. Strong **directional dependence** (σx vs σy) observed, consistent with welding-induced anisotropy.
- Data validation confirms repeatability and consistency across measurements.

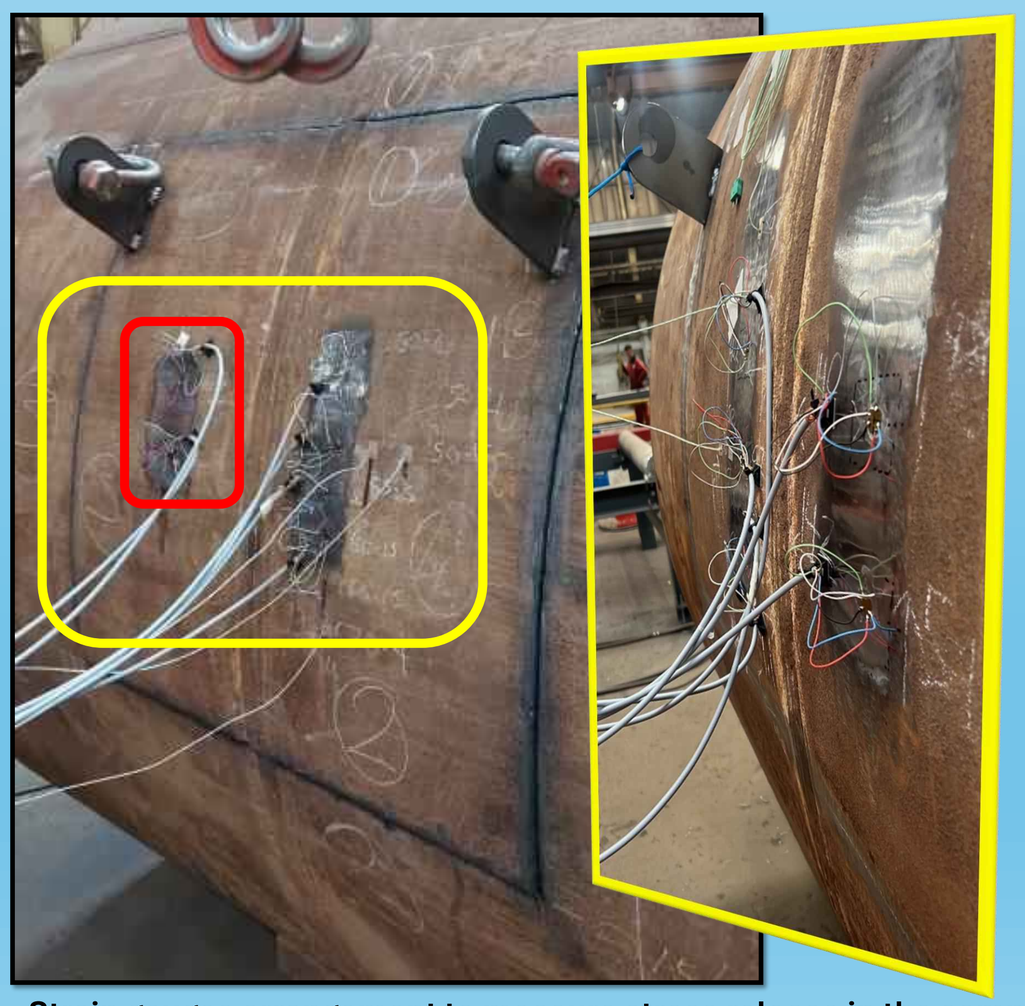

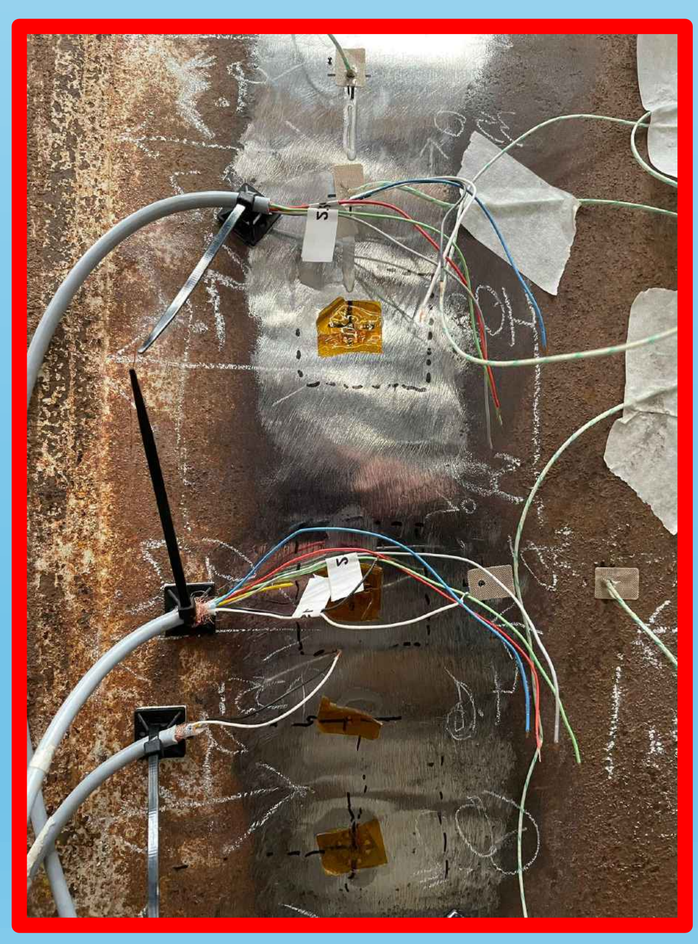

Strain gauges arrangement to measure stress release in the samples during the cutting procedure

This work was supported by the Supergen ORE Impact Hub Flexible Funding under Grant EP/Y016297/1 from the UK Engineering and Physical Sciences Research Council (EPSRC).

An Integrated Experimental–Computational Framework for Erosion Analysis of Tidal Turbine Blades

Payvand Habibi, Ali Mehmanparast, Saeid Lotfian

Department of Naval Architecture, Ocean & Marine Engineering (NAOME), Faculty of Engineering, Glasgow, UK

Abstract

Tidal turbine blades in sediment-laden environments experience slurry erosion, reducing performance and durability. This study develops an integrated experimental–computational framework combining FR4 erosion testing with CFD-based calibration of the Oka model. Applied to a NACA63-415 hydrofoil, the method predicts erosion-induced roughness distributions and supports improved blade design and lifetime assessment.

Introduction

Tidal turbine blades in sediment-laden environments suffer slurry erosion that degrades performance [1, 2]. Although GFRP composites are widely used, their erosion behaviour remains insufficiently understood. This study investigates FR4 erosion using an integrated experimental–computational framework linking testing, particle tracking, and Oka model predictions to surface roughness evolution.

Methodology

1. Slurry erosion testing

Accelerated slurry jet tests (100–150 μm sand, 12.5 m/s) were used to simulate marine conditions, with **erosion** quantified by **mass loss** [3].

1. 2. Surface analysis Optical profilometry

was used to assess surface **roughness** evolution and erosion **morphology** [4].

1. 3. CFD and erosion modelling

CFD-based **particle tracking** provided impact conditions to calibrate the Oka erosion model for composite materials [5].

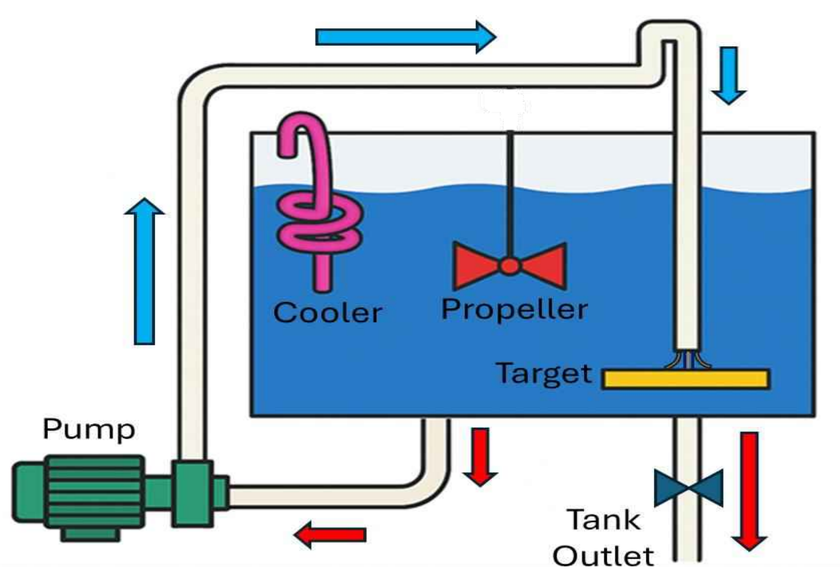

Schematic Diagram of Slurry Erosion Impingement Rig.

Results

1. Erosion behaviour:
FR4 showed **mixed ductile–brittle mechanisms**, with peak erosion near 60° impact angle [6].

2. Material degradation trend:
Mass loss increased approximately **linearly** with time, indicating a **stable erosion rate**.

3. Surface degradation relationship:
A strong **linear correlation** was found between **roughness rate (Rz) and mass loss rate**, enabling estimation of erosion severity from surface measurements:

$$\dot{R}_z = 3038.69 \times (\textit{Mass loss rate}) + 19.21$$

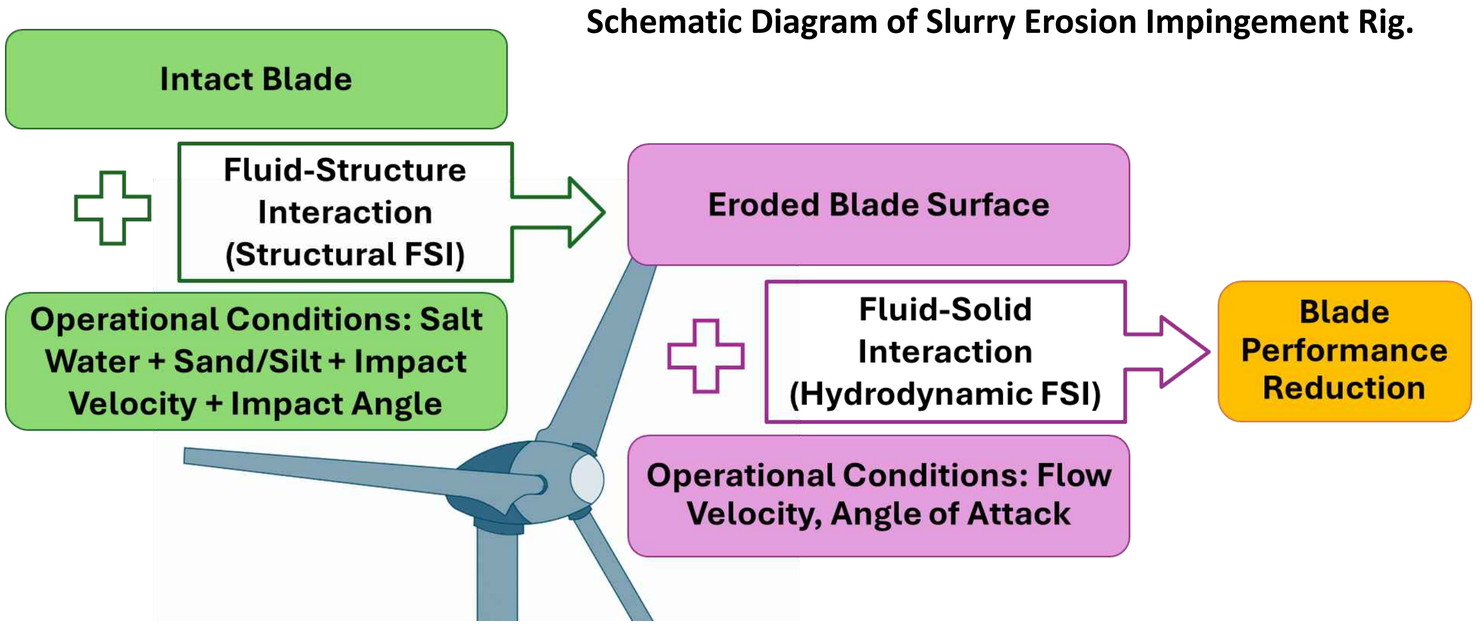

The Process of Erosion initiation and Propagation on a tidal Blade

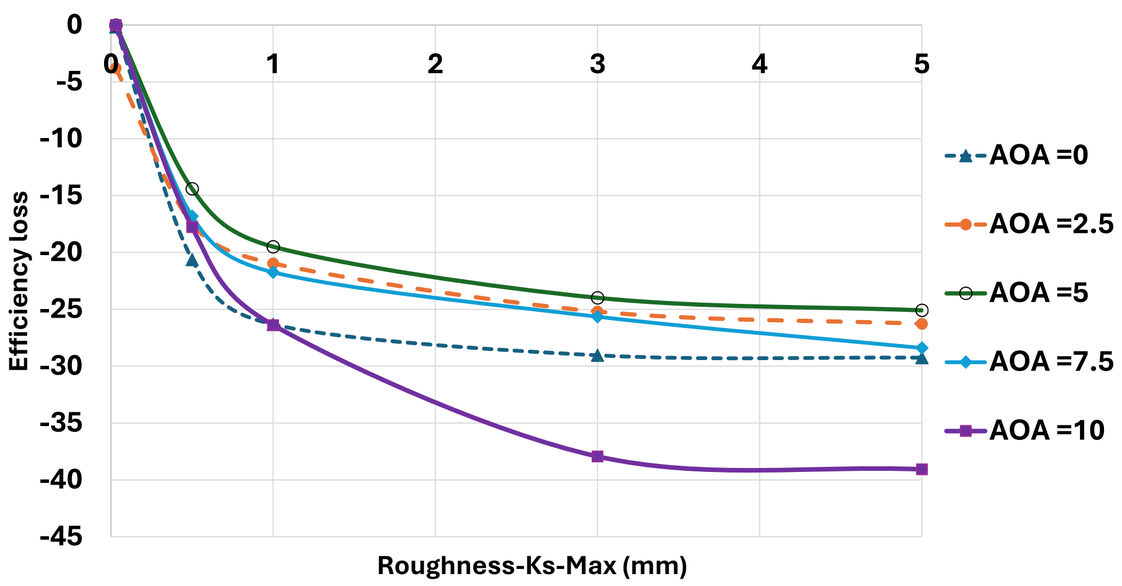

Efficiency vs. Max Roughness Height

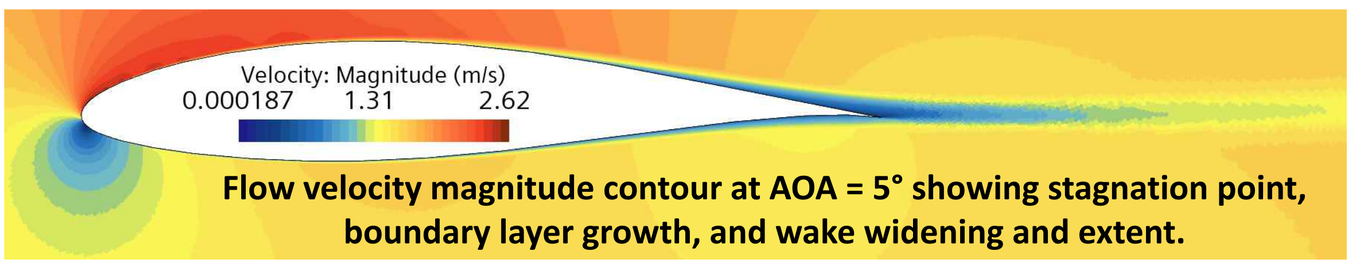

Flow velocity magnitude contour at AOA = 5° showing stagnation point, boundary layer growth, and wake widening and extent.

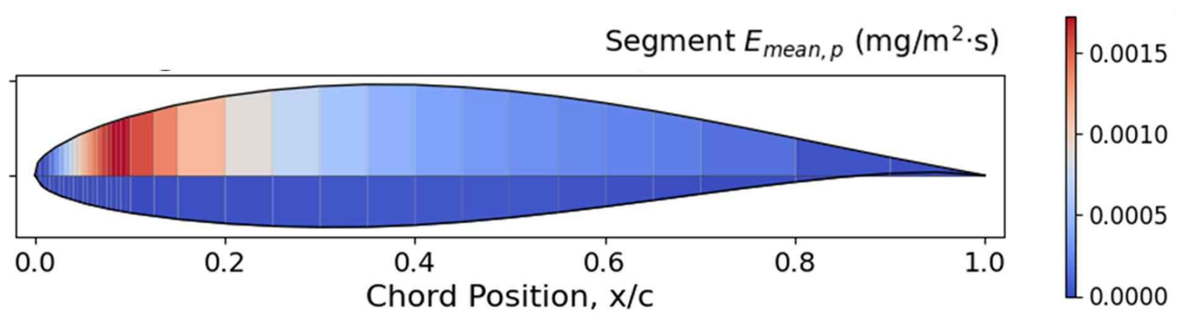

Heatmap of Mean Erosion Rate on a NACA 63-415 at Re=1.6e6, AOA=5deg.

Conclusions

1. A robust integrated framework combining **experiments**, **surface analysis**, and **CFD** was developed for tidal turbine blade erosion.

2. The approach is transferable to **different materials**, **geometries**, and **operating conditions**.

3. It enables reliable **prediction of erosion** behaviour, supporting improved **blade design**, **durability**, and **maintenance planning**.

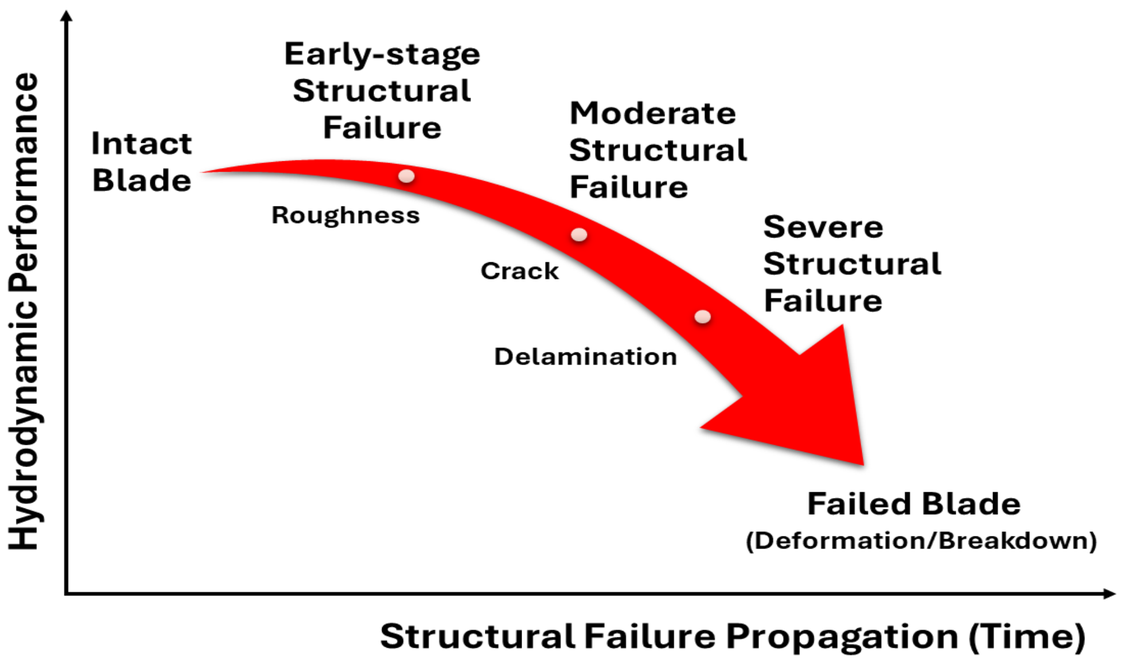

General Behaviour of the Blade Performance Against Structural Failure.

References

[1] **Wood**, R. J. K. Erosion–corrosion interactions and their effect on marine materials; 2006; [2] **Habibi**, P. et al. Failure analysis of tidal turbine blades: understanding erosion mechanisms and their impact on structural integrity; 2025; [3] **Habibi**, P. et al. Correlation between erosion-induced roughness and mass loss in FR4 composites; 2025; [4] **Oka**, Y. et al. Practical estimation of erosion damage caused by solid particle impact; 2005; [5] **Biswas**, S., Satapathy, A., Patnaik, A. Erosion wear behaviour of polymer composites: a review; 2010; [6] **Bitter**, J. A study of erosion phenomena; 1963.

Scan me!

Unsteady hydrodynamic forces on a forced oscillating rotor

Yadong Han[1], Nijmeh Marouf[1], Ross Calvert[2], Federico Zilic de Arcos[1], Amanda Smyth[1], Christopher Vogel[1], Richard Willden[1]

[1] Department of Engineering Science, University of Oxford, [2] School of Engineering, University of Edinburgh

Introduction

➢ **Motivation**

- Floating tidal turbines experience **platform motions**, leading to highly **unsteady hydrodynamic loads**.
- The impact of platform motion on **turbine performance** and **unsteady loading** is still unclear.
- Reliable prediction of **added mass** and **damping** effects is essential for accurate numerical modelling.

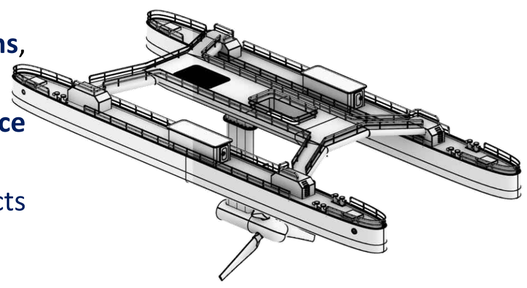

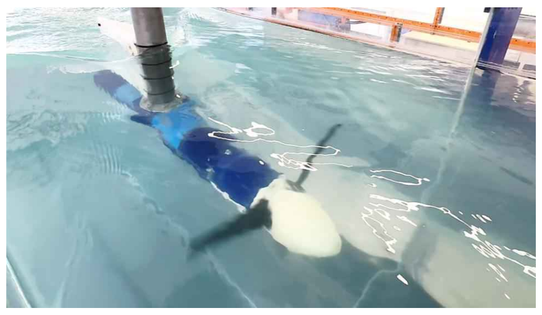

➢ **Objectives**

- Understand how **surge motion** affects turbine performance and blade loads.
- Quantify **added mass** and **damping** effects.
- Support the development and **validation** of **numerical models**.

Experimental Methodology

➢ **Turbine Model and Instrumentation**

- Rotor diameter: 0.06m
- Design tip-speed ratio: $\lambda = 5$
- Renolds number: 1.2×10^5
- Thrust / toque transducers
- Root bending moment sensors
- Rotary encoder

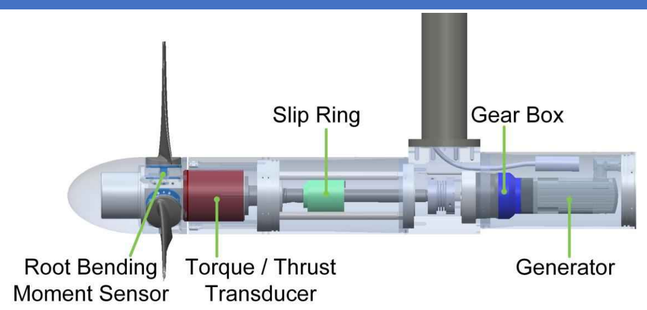

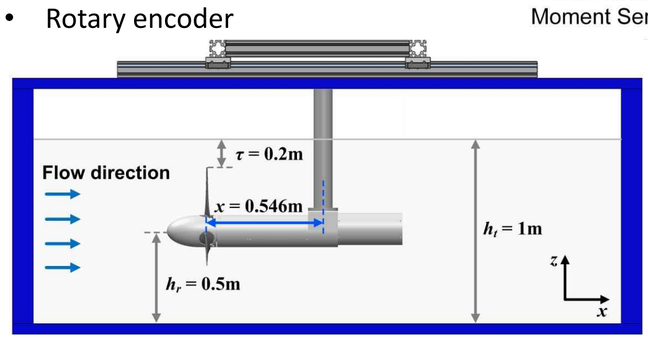

➢ **Flume and Surge Motion Rigs**

- Flume size: 10m×1.1m×1m
- Inflow velocity: 0.575 m/s
- Turbulence intensity: 2%
- Blockage ratio: 25.7%
- Maximum stroke length: 76mm
- Surge frequency: 0 – 3 Hz

Surge Motion and Load Response

- The imposed surge motion is accurately reproduced, with measured displacement closely matching the prescribed sinusoidal signal.
- Both thrust and torque exhibit clear sinusoidal variations, indicating a consistent dynamic response to the imposed motion.
- The **dominant frequency** in all signals corresponds to the **surge frequency** f_s.

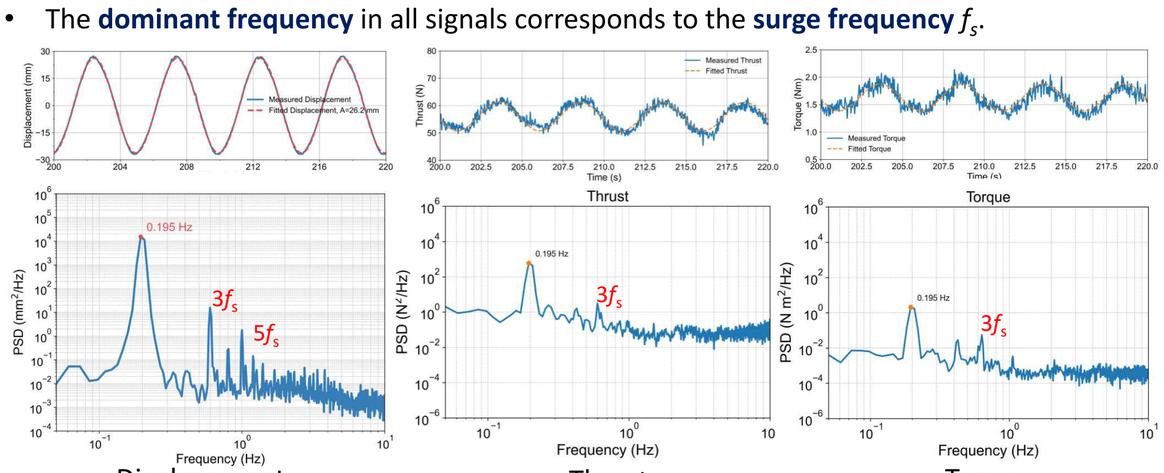

Displacement Thrust Toque

Time-averaged Thrust and Torque

- **Mean power increases slightly** with increasing surge amplitude, with a tendency for stronger enhancement at lower frequencies.
- **Mean thrust** shows a consistent but **modest increase** across all tested conditions.
- The variation remains within 10%, indicating **limited impact on time-averaged performance**.

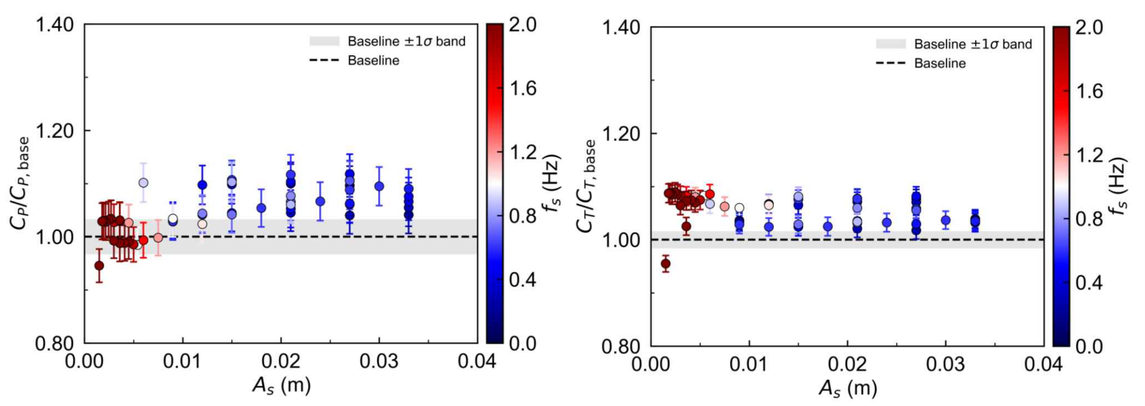

Mean power coefficient Mean thrust coefficient

Dependence of Unsteady Loading on Current Number

- **Current number:** $\mu = \dfrac{\omega_s A_s}{U_c}$

  where ω_s is the surge frequency, A_s is the surge amplitude, and U_c is the inflow velocity.
- The **current number** provides a **unified scaling parameter** for load fluctuations, combining the effects of surge amplitude and frequency.
- **Fluctuation amplitudes** exhibit a **strong linear dependence on current number** μ.
- **Edgewise load fluctuations** exhibit approximately **twice** the magnitude of **flapwise fluctuations** at the same current number.
- At current number μ = 0.2, the **edgewise load** increases by approximately **60%**, while the **flapwise load** increases by about **30%**.

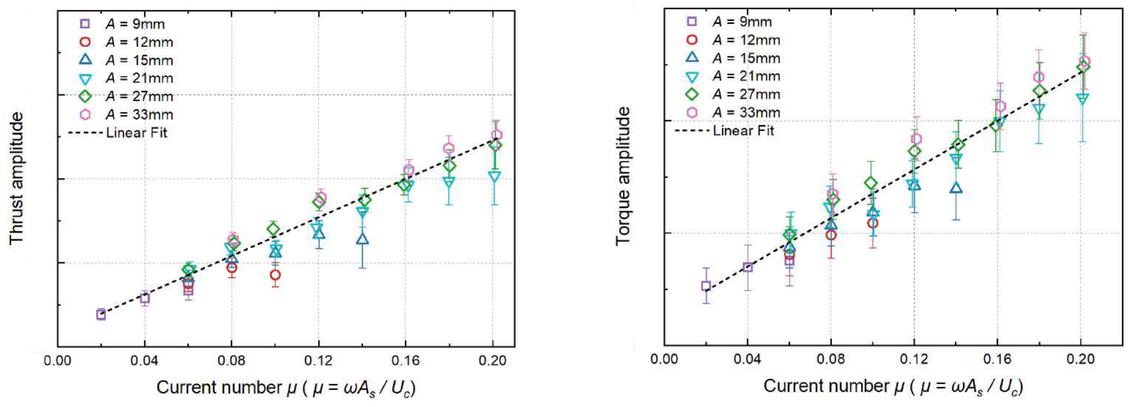

Thrust and torque fluctuation amplitudes vs current number

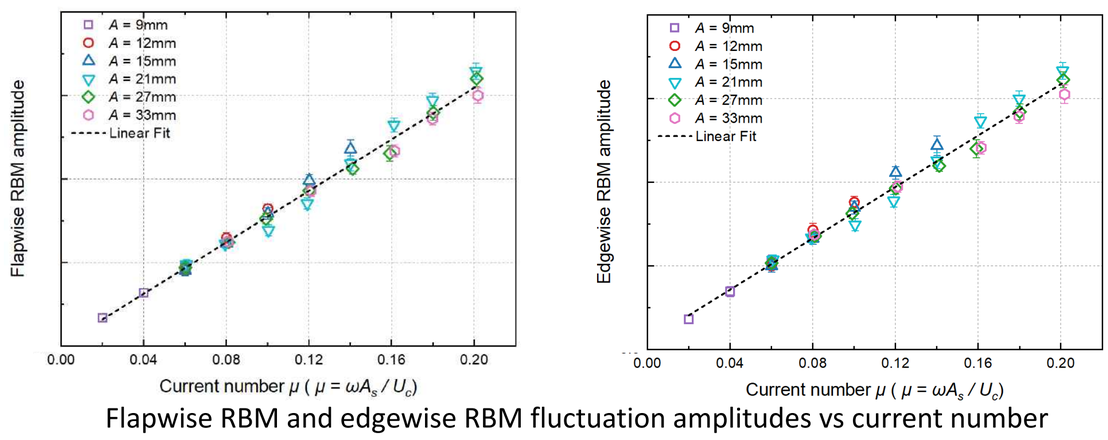

Flapwise RBM and edgewise RBM fluctuation amplitudes vs current number

Dependence of Added Mass and Damping on Frequency Ratio

- **Frequency ratio:** $f^* = \dfrac{\omega_s}{\omega_r}$ where ω_r is the rotational frequency.
- C_v' and C_A' denote the damping and added mass coefficients, respectively.
- The **added mass** and **damping coefficients** collapse onto a **single trend across different current numbers**, indicating that frequency ratio is the dominant parameter.
- The **damping coefficient** shows a **non-monotonic trend** with frequency ratio, with a local reduction around frequency ratio 0.6.
- The **added mass coefficient** increases approximately **linearly** at low frequency ratio, and then **approaches a constant value**.
- The **added mass remains significantly smaller than damping**, indicating that damping dominates the unsteady load response.

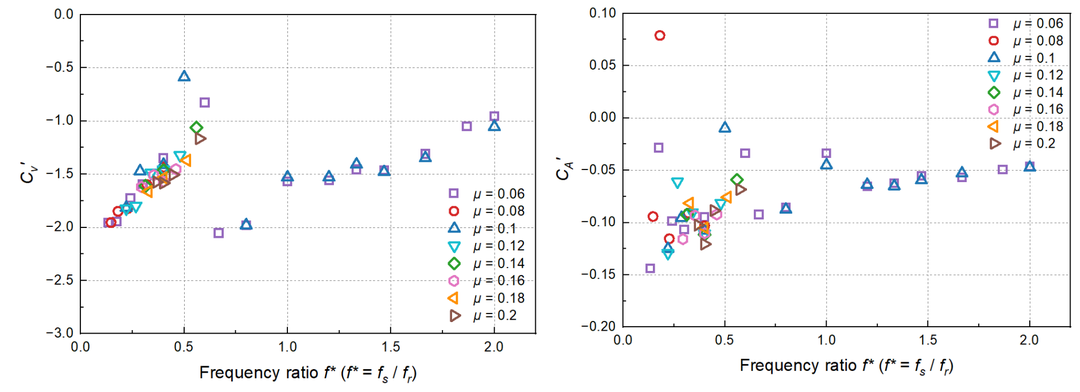

Added mass and damping coefficients of thrust

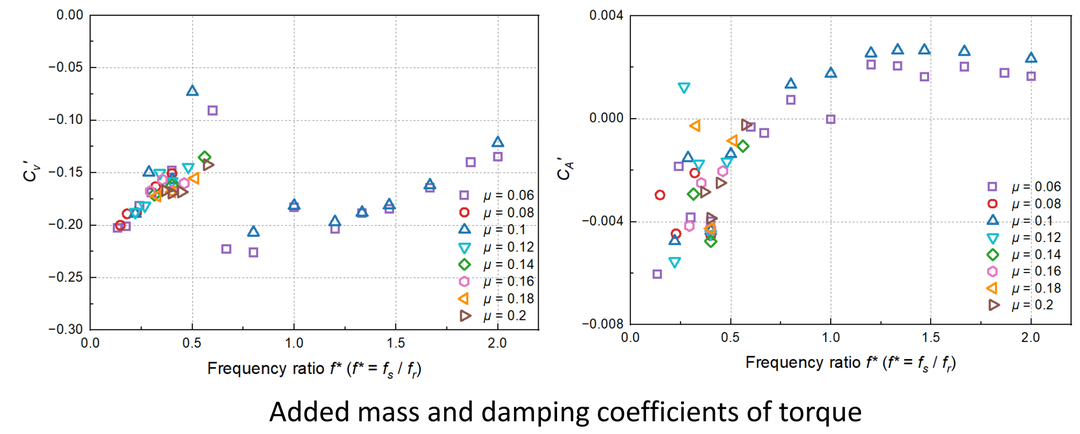

Added mass and damping coefficients of torque

Acknowledgements

- We would like to acknowledge the financial support of SuperGen ORE Hub EP/Y016297/1, RHJW's EPSRC Advanced Fellowship EP/R007322/1, and EPSRC Co-Tide EP/X03903X/1.

Assessing the **contribution of VIV** to *fatigue damage* in dynamic power cables

This study, as part of the CableDyn project, is investigating whether vortex-induced vibration (VIV) poses a significant fatigue damage risk to dynamic power cables on floating offshore wind turbines. Using scaled physical experiments at the FloWave facility, three-dimensional cable motion was tracked under isolated and combined wave and current loading. Fatigue damage was estimated from curvature time histories using Miner's rule, and the relative contributions to fatigue damage of VIV and wave-induced motion have been assessed across different loading conditions and directions.

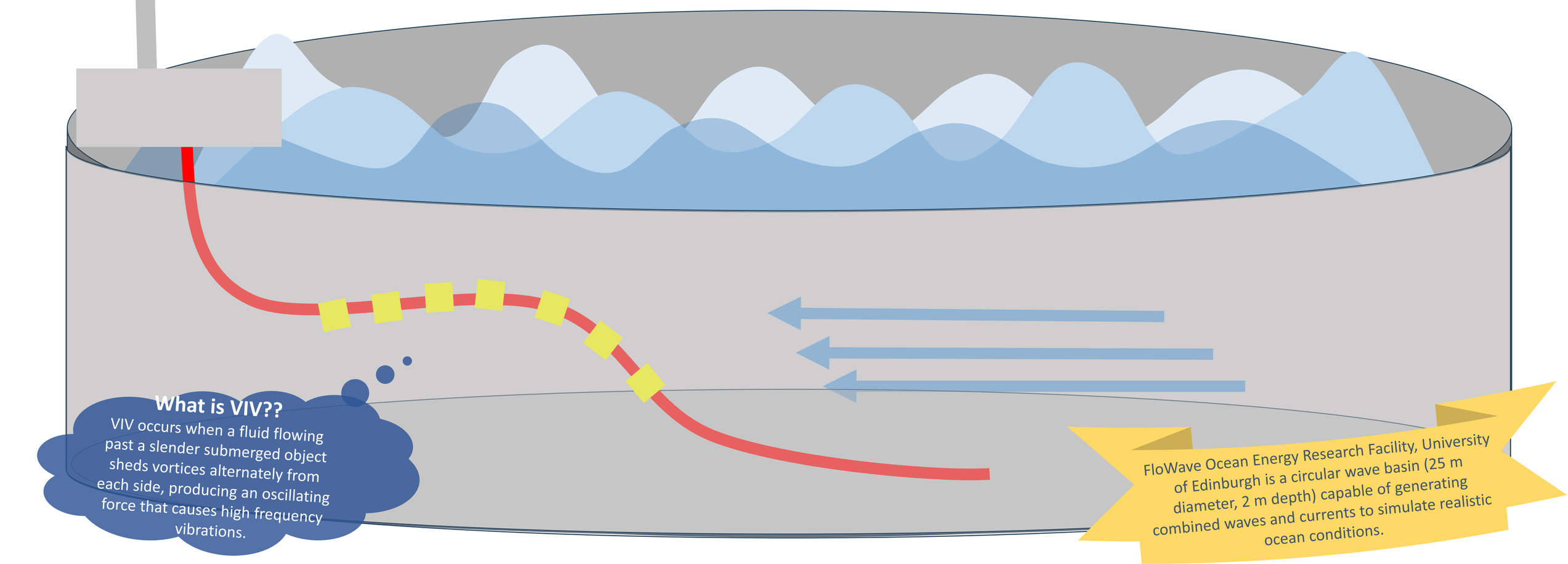

EXPERIMENTS

- **A 1:50 scale model of a dynamic power cable** for an offshore wind turbine power cable was developed (figs. 1 and 2)
- The cable model was 31mm in diameter, 5m long, and was comprised of an inner 3-core power cable (9.8 mm diameter), 3D-printed spacers at 2 mm intervals, and an outer silicone tube. Strain gauges were embedded throughout.
- **Cable motion was captured** using an underwater Qualisys motion tracking system, with 37 markers **affixed at 100mm intervals** along the cable exterior.
- Tests covered **wave-only, current-only, and combined wave-current** loading conditions.

FATIGUE DAMAGE ESTIMATION

1. XYZ Qualisys data of each marker used to estimate curvature along the cable, using method of finite differences to obtain derivatives between markers

2. Curvature (κ) related to stress (σ) by Young's modulus (E) and cable radius (r):

$$\sigma(t) = E \cdot \varepsilon(t) = E \cdot r \cdot \kappa(t)$$

3. Stress cycles (n_i) counted using Rainflow analysis

4. Damage (D) per test estimated using Miner's rule:

$$D = \sum_{i=1}^{k} \frac{n_i}{N_i}$$

Where N_i is the number of cycles to failure

3. And from Basquin's approximation damage is estimated as:

$$D \propto \sum_{i=1}^{k} n_i \sigma_i^m \propto \sum_{i=1}^{k} n_i \kappa_i^m$$

For some constants C and m

KEY PRELIMINARY RESULTS

- 30 degrees offset worst direction for current only (fig.3)
- Generally, higher current speeds cause more VIV and therefore higher fatigue damage (fig. 3)
- However, fatigue damage not monotonically related to current speed (fig. 3)
- Fatigue damage due to combined loading is similar to current only results, indicating a more significant contribution of fatigue damage from VIV than waves (fig. 4)

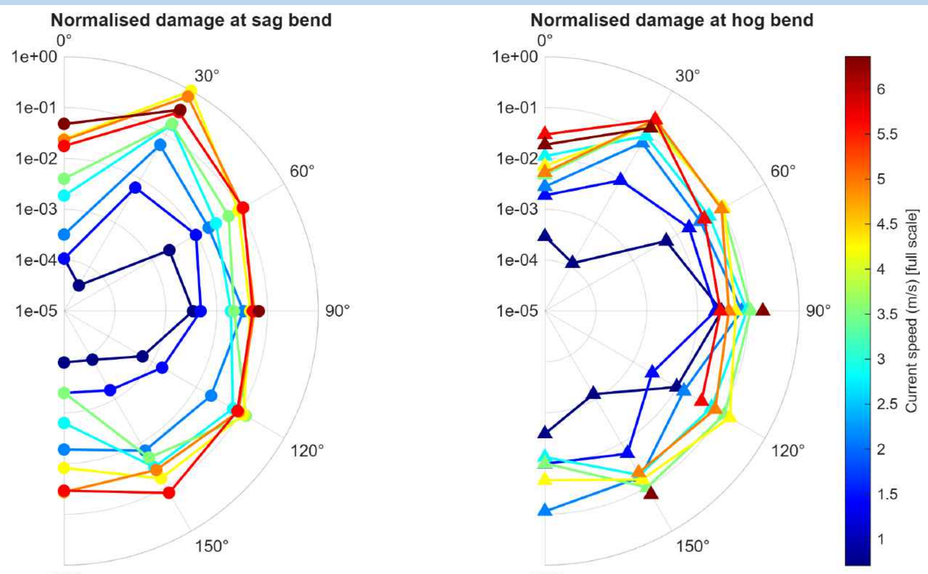

Figure 3: Radial plots showing the relative magnitude of fatigue damage caused by VIV for different current speeds and directions (cable laid 0-180°)

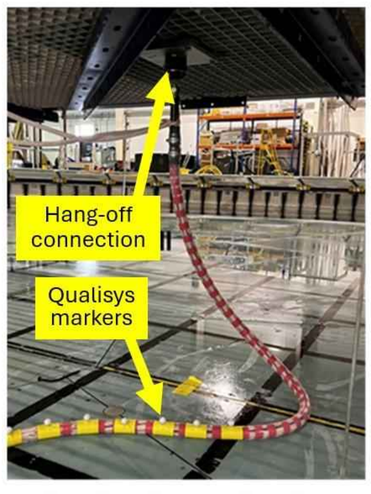

Figure 1: Cable model in FloWave lab

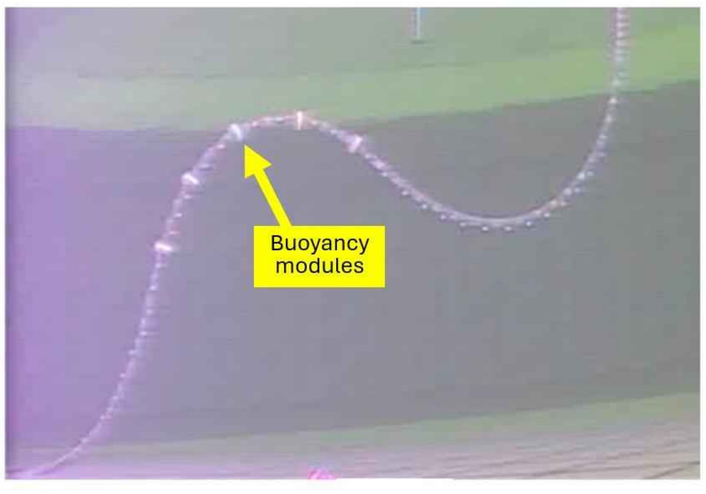

Figure 2: Cable model underwater in FloWave ocean basin

DISCUSSION

- The combined case indicates that VIV is a significant contributor to fatigue damage, but **the current speeds tested were much higher than realistic floating offshore wind sites** and therefore further work should be done to determine whether VIV is an issue for dynamic power cables for floating offshore wind.
- For dynamic power cables that might experience high current speeds, such as floating tidal devices, **VIV suppression techniques such as strakes** can be applied, which disrupt the flow around the cable.

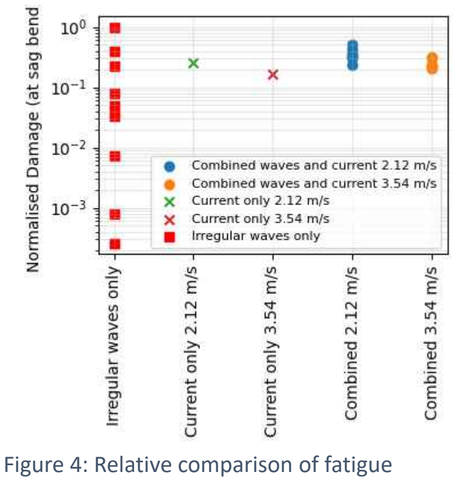

Figure 4: Relative comparison of fatigue damage caused by wave-only loading, current-only and combined wave and current loading (all loading at 90° to cable) [full scale]

Anna Holcombe[1], Ed Mackay[1], Philipp Thies[1], Faryal Khalid[1], Venki Venugopal[2]

[1] University of Exeter, Penryn, UK

[2]University of Edinburgh, UK

a.r.holcombe@exeter.ac.uk

Reduced-Order Modelling of Tidal Turbine Rotor Blade Structures

Name: Sam Hughes
Supervisor(s): Prof. Dilum Fernando, Dr. Eddie McCarthy, Dr. Gabrielis Cerniauskas

Wind & Marine Energy Systems CDT, Rm 3.36, Royal College Building
University of Strathclyde, 204 George Street, Glasgow, G1 1XW
samuel.hughes@ed.ac.uk

1. Objectives

- *Develop an inverse design screen* and *performance analysis* methodology for tidal blade structures
- Utilise the principle of equivalent stiffness to build equivalent structures
- Include *serviceability, ultimate, buckling and fatigue limit state constraints* into the framework
- Introduce dependencies on database information which improves with experience and further study

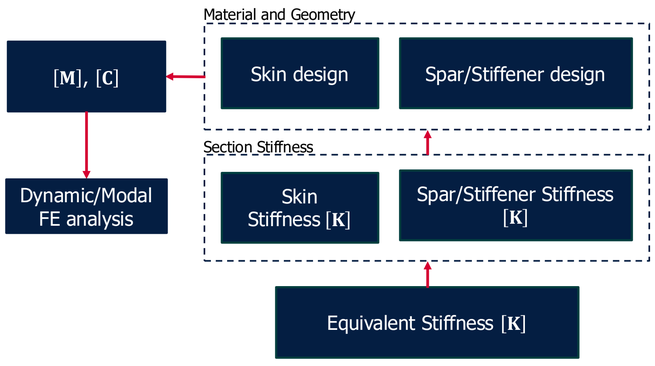

Why a low order sweep?
- Early discard of non-viable structural solutions
- Bounds detailed structural design problem space

Iteration step $\mathbf{K}_i \rightarrow \mathbf{K}_{i+1} = \mathbf{F}_{beam}\mathbf{U}$ *virtual*

Step error matrix $\Delta\mathbf{K}_e = \mathbf{K}_{e,i} - \mathbf{K}_{e,i+1}$

Equivalent stiffness $[\mathbf{K}] = \sum_{i=1}^{n} \mathbf{K}_i$

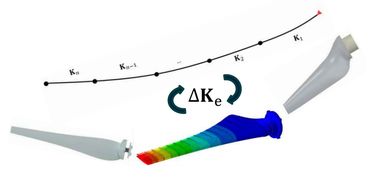

1D Stiffness Selection

Allowable stress: $\sigma_{allow} = \sigma_{us}\frac{\alpha}{FoS}$

i. α = geometric strength reduction
ii. FoS = material strength factor of safety

Condition 1: $\frac{M_{YB}(Z)X}{I} < \sigma_{us}\frac{\alpha}{FoS}$

Condition 2: $\min \int EI(z/L)$

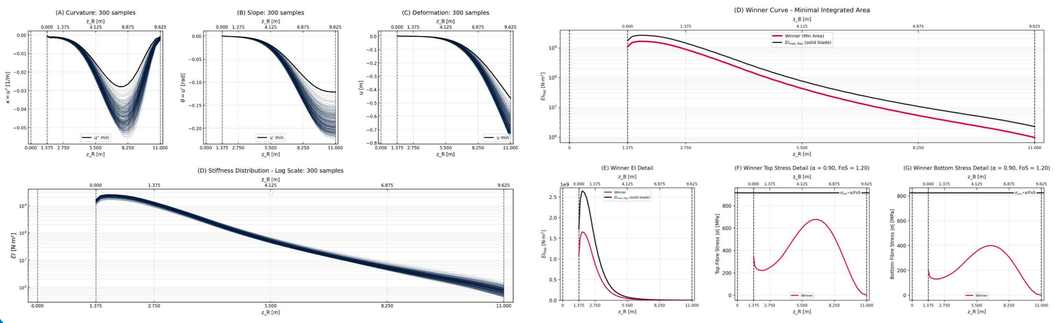

2D Stiffness Selection

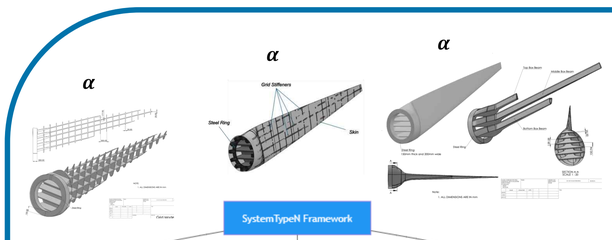

SystemType{X}{Y}-{Z}

Symbol	Meaning	Values
X	Number of webs	0, 1, 2, 3, 4, ...
Y	Spar cap configuration	A = none, B = fixed, C = box
Z	Web orientation	CN = chord-normal, F = flapwise *(omitted when X = 0)*

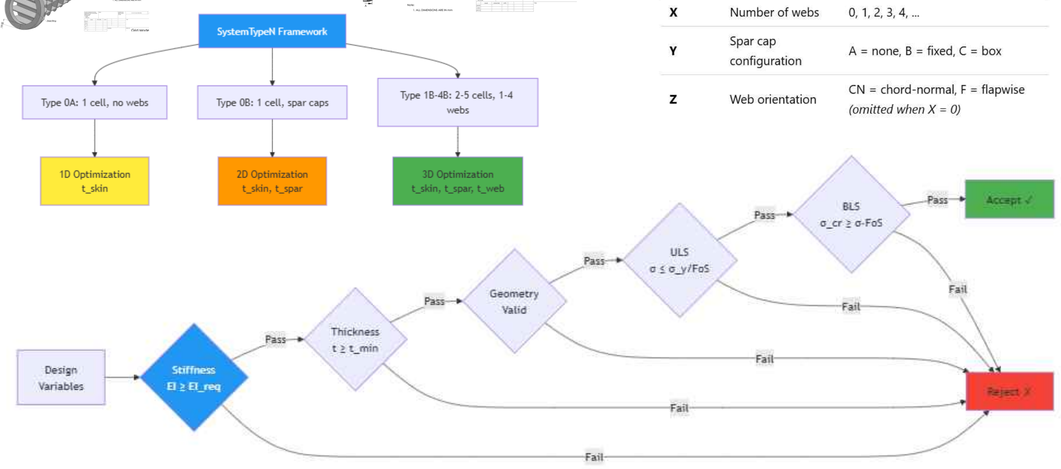

Structural System Types: B-Frame Normalized Cross-Sections (SystemType{X}{Y}-{Z})

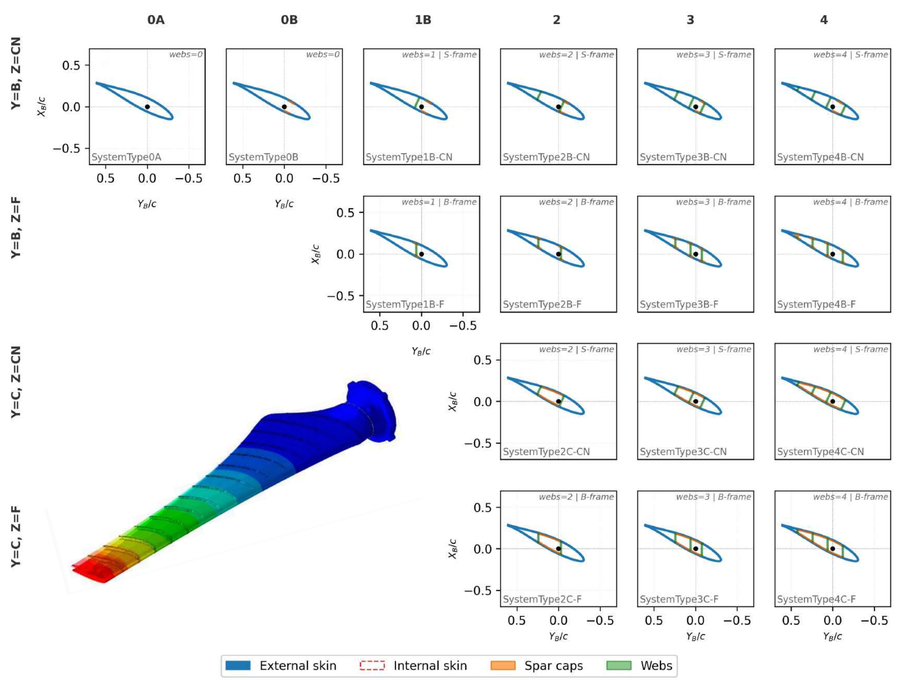

B-frame normalized: +X_B up, +Y_B left: LE right, suction top. Rows: Y, Z (SystemType{X}{Y}-{Z}). Cols: 0A, 0B, 1B, then X=2,3,4 (Y from row).

Chord: 1.3m | Twist: 25°

Blade External Geometry and internal Forces

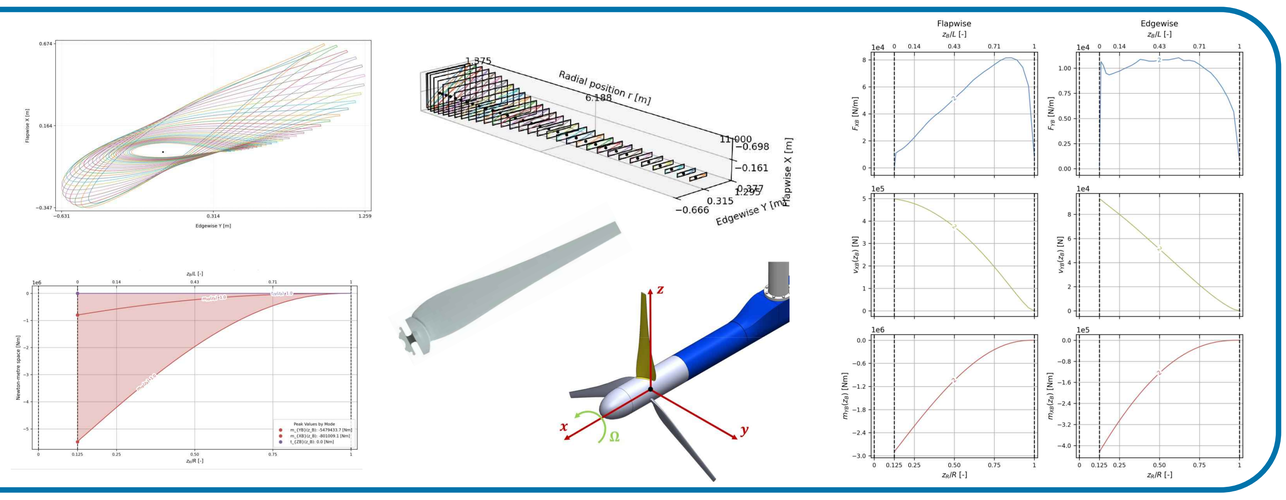

DIC 1D Stiffness

FloWave testing campaign

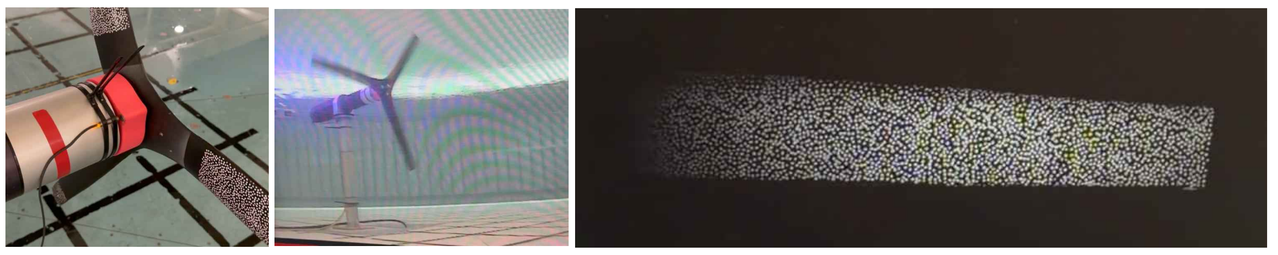

Structural Design Envelope Feasibility

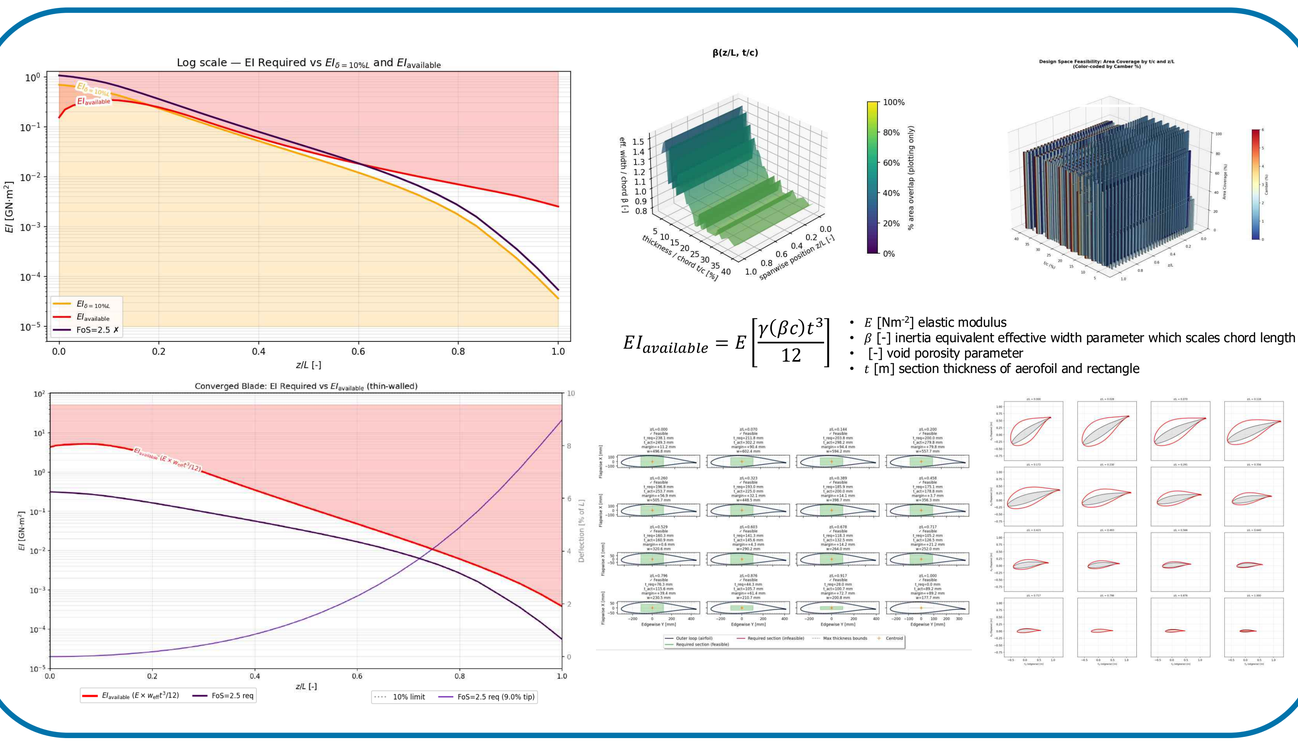

$$EI_{available} = E\left[\frac{\gamma(\beta c)t^3}{12}\right]$$

- E [Nm^{-2}] elastic modulus
- β [-] inertia equivalent effective width parameter which scales chord length
- γ [-] void porosity parameter
- t [m] section thickness of aerofoil and rectangle

Fatigue Limit State

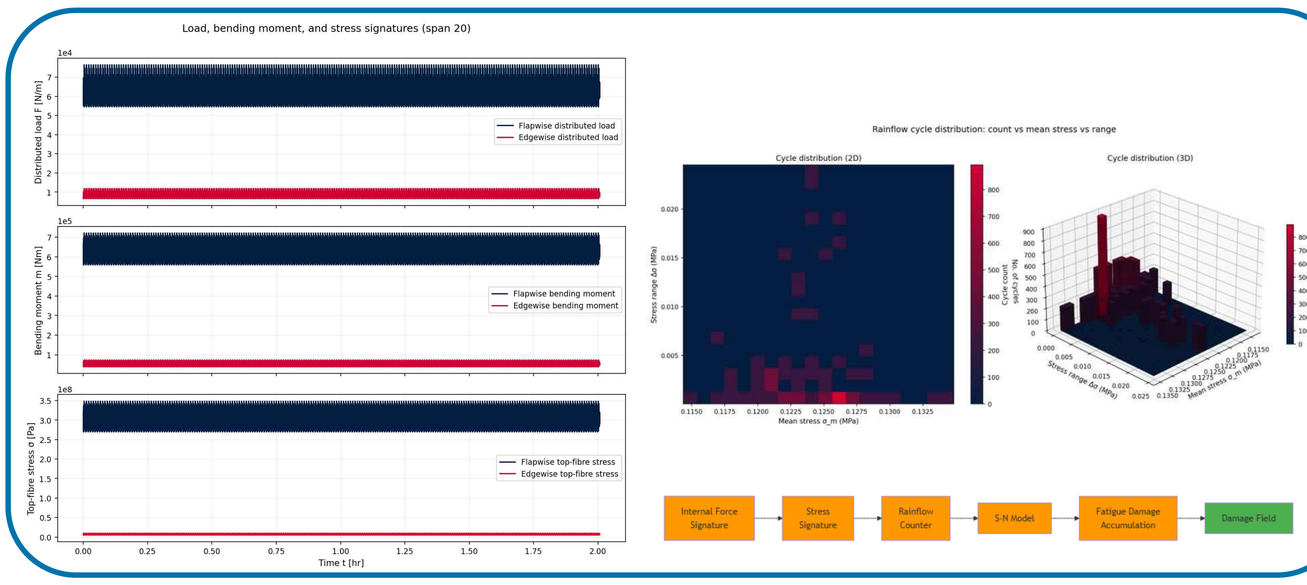

Next Steps and References

- *2D stress* verification framework shear flow equations, *PreComp NREL and CBCSA*
- *2D buckling* verification framework
- *Equivalent laminate model* for subcomponent j: $E_j = E_{equ}(n)$ or $E_{equ}(n,\theta)$

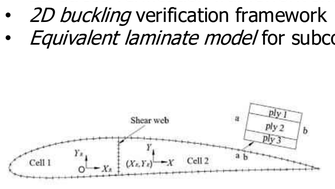

Fig. 6. Discretization of a typical blade cross-section with one shear web.

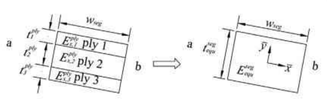

Fig. 7. Equivalent representations of area segment.

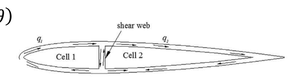

Fig. 3. Blade cross-section with one shear web.

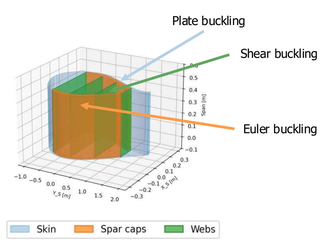

Engineering and Physical Sciences Research Council

THE UNIVERSITY of EDINBURGH
Institute for Infrastructure and Environment